Astronomical Techniques and Instruments, Vol. 3, May 2026, 1–12

Article Open Access

PyTransHelio: A Python tool for analyzing magnetic flux-weighted centroids of active regions and trans-equatorial loop footpoints in full-disk solar photospheric magnetograms

Silin Liu[1,2], Jie Chen[2*], Zechen Wen[2,3], Marianna B. Korsós[4,5,6], Robertus Erdélyi[5,6,7], Chenfei Zhao[2,8], Zihan Yu[9], Ying Song[1]

[1]*Beijing Information Science and Technology University*, *Beijing* 102200, *China*

[2]*Key Laboratory of Solar Activity and Space Weather*, *National Space Science Center*, *Chinese Academy of Sciences*, *Beijing* 100190, *China*

[3]*Beijing Normal University*, *Beijing* 100875, *China*

[4]*University of Sheffield*, *School of Electrical and Electronic Engineering*, *Sheffield S*1 3JD, *UK*

[5]*Solar Physics and Space Plasma Research Centre, School of Mathematical and Physical Sciences, University of Sheffield* S3 7RH, *UK*

[6]*Department of Astronomy*, *Eötvös Loránd University*, *Budapest* 1112, *Hungary*

[7]*Gyula Bay Zoltán Solar Observatory (GSO)*, *Hungarian Solar Physics Foundation (HSPF)*, *Gyula* 5700, *Hungary*

[8]*Jilin University*, *Jilin* 130015, *China*

[9]*University of Electronic Science and Technology of China*, *Chengdu* 610000, *China*

*Correspondence: chenjie@bao.ac.cn

Received: August 22, 2025; Accepted: September 26, 2025; Published Online: September 29, 2025; https://doi.org/10.3724/ati2025068; https://cstr.cn/32083.14.ati2025068

Citation: Liu, S. L., Chen, J., Wen, Z. C., et al. 2026. PyTransHelio: A Python tool for analyzing magnetic flux-weighted centroids of active regions and trans-equatorial loop footpoints in full-disk solar photospheric magnetograms. *Astronomical Techniques and Instruments*, **3**(3): 1−12. https://doi.org/10.3724/ati2025068.

Abstract: This paper introduces PyTransHelio, a Python-based graphical interface tool designed for solar physics research, which automates the calculation of magnetic flux-weighted centroid coordinates of active regions in full-disk magnetograms and supports the identification and analysis of footpoints in trans-equatorial loops. The tool addresses the operational complexity and lack of dedicated graphical user environments in traditional Interactive Data Language/SolarSoftWare workflows by integrating modules for magnetogram header parsing, three-coordinate system conversions (pixel/Stonyhurst/Carrington coordinates), automatic magnetic pole detection, and footpoint distance calculation, enabling end-to-end automation. Users can swiftly obtain active region centroid positions and trans-equatorial loop footpoint spacings through an intuitive three-step workflow: "Load → Click → Results." Its modular architecture balances flexibility and extensibility as an open-source tool, significantly lowering the barrier to solar photospheric magnetogram analysis.

Keywords: Active regions; Trans-equatorial loops; Full-disk magnetograms; Open-source tool; Graphical user interface

1. INTRODUCTION

Sunspots, the most visible manifestations of solar magnetic activity, have been central to humanity's exploration of solar physics since Galileo's era. They represent the "footprints" of intense magnetic flux tubes penetrating the solar photosphere, which often converge to form larger-scale magnetic structures known as active regions (ARs). These ARs serve as the core building blocks for energy storage and release in the solar atmosphere, giving rise to violent energy eruptions such as solar flares, coronal mass ejections (CMEs), and solar energetic particle events. Historically notable ARs, such as the source region of the 1859 "Carrington Event" or the AR cluster during the 2003 Halloween storms, starkly demonstrate the potentially catastrophic impact of extreme AR eruptions on Earth's space environment and modern technological systems[1]. Studying the physical properties, evolutionary patterns, and eruptive potential of ARs is not only key to understanding the nature of solar magnetic activ-

ity but also foundational for assessing their heliospheric effects[2].

The Sun follows an approximately 11-year activity cycle. Since December 2020, it has entered Solar Cycle (SC) 25. According to the latest predictions and observations from international authorities, the current cycle is expected to peak between 2024 and 2025[3]. During this peak phase, the likelihood of super ARs–characterized by greater numbers, larger sizes, and more complex magnetic configurations–emerging on the solar surface increases significantly. Eruptions from such super ARs, including intense flares and high-speed CMEs, can severely perturb interplanetary space and Earth's magnetosphere, triggering catastrophic geomagnetic storms, upper atmospheric heating, radiation belt electron acceleration, satellite orbital decay, and even power grid failures[4]. Against this backdrop, the need for precise characterization and dynamic monitoring of ARs has become more urgent than ever[3,5].

The internal magnetic structure of ARs is often highly inhomogeneous and asymmetric. Traditional morphological descriptors (e.g., contour-based centroids) may fail to capture their physical center, particularly in cases of bipolar/multipolar interactions, trans-equatorial AR complexes, or coronal loop footpoint localization[6]. To overcome this limitation, we have developed a magnetic flux-weighted centroid algorithm for ARs based on full-disk longitudinal magnetogram data. The algorithm uses high-resolution, continuous-coverage photospheric magnetograms from the Solar and Heliospheric Observatory (SOHO) /Michelson Doppler Imager (MDI) and the Solar Dynamics Observatory/Helioseismic and Magnetic Imager (SDO/HMI) instruments[7]. It uses the magnitude of the vector magnetic field at each pixel as a weighting factor, to compute the centroid of AR magnetic distributions. This method shifts focus from morphological edges to the spatial core of magnetic flux concentration, offering a more objective representation of AR "magnetic centers"[4].

Calculating magnetic flux-weighted centroids for ARs holds significant practical value. Firstly, it provides a unified, quantifiable metric for locating core magnetic structures, facilitating quantitative analysis of internal AR configurations and cross-AR comparisons. More critically, precise centroid calculations and their associated photospheric footpoint positions are essential for quantifying cross-equatorial flux transport efficiency and large-scale loop system extensions in studies of trans-equatorial ARs or interconnected coronal loop systems, e.g., footpoint localization of trans-equatorial loops (TLs). These metrics are vital for understanding global solar magnetic coupling, energy transfer pathways, and predicting the impact scope of potential eruption sources[8].

TLs are large-scale bright loop structures spanning the solar equator to connect both hemispheres, first observed during the Skylab mission in the 1970s. These structures average 20°–30° in longitudinal extent (up to 61° at maximum) and are widely attributed to magnetic reconnection–when magnetic field lines from ARs in opposite hemispheres extend to equatorial regions, forming cross-hemispheric linkages via X- or Y-type reconnection. TLs are not only correlated with the SC (~35% of ARs exhibit such connections), but also dynamically linked to flares and CMEs; they may vanish due to flare-induced destabilization or trigger CMEs upon eruption. Within solar dynamo theory, TLs are regarded as key structures sustaining cross-hemispheric magnetic coupling, critical for understanding the poloidal-toroidal field conversion mechanism. Recent decade-long observations by the X-Ray Telescope (XRT) aboard the Hinode solar observatory spacecraft (Hinode/XRT) have provided a robust statistical foundation for TL research[9,10]. When TLs link ARs across hemispheres, accurately measuring the distance between their opposite-polarity footpoints (i.e., the magnetic flux-weighted centroids of the connected ARs) becomes a key metric for studying large-scale magnetic coupling.

Current research in this field heavily relies on the Interactive Data Language/SolarSoftWare (IDL/SSW) toolchain, which poses notable bottlenecks: the workflow is cumbersome, requiring manual integration of multiple standalone tools for coordinate conversions (pixel → Stonyhurst → Carrington) and centroid calculations; the command-line-driven approach entails a steep learning curve, hindering accessibility for non-specialists, and; the lack of visual interactivity prevents intuitive guidance during analysis. Although Python ecosystems (e.g., sunpy, drms) offer solar data interfaces, end-user-oriented, integrated graphical user interface (GUI) tools remain scarce.

To address these challenges, we developed PyTransHelio. The tool introduces valuable integrated functionalities: a one-click pipeline automating magnetogram header parsing, multi-coordinate conversions, magnetic pole identification, centroid computation, and TL footpoint pairing with spacing outputs. Simultaneously, PyTransHelio offers an interactive GUI, enabling users to locate ARs via region selection or clicks, visualize magnetic pole weight distributions and centroids in real time, and annotate TL footpoint pairs with connecting lines. Designed as an efficient, user-friendly all-in-one solution, PyTransHelio can work in both core solar physics research (e.g., magnetic topology modeling) and educational applications.

2. TECHNIQUES AND METHODS

The core processing pipeline (see Fig. 1) of PyTransHelio begins with magnetogram file input, supporting flexible image transport system (FITS) format data from SOHO/MDI and SDO/HMI. Key header information (observation time, resolution, instrument parameters) is first extracted via the astropy.io.fits module. Subsequently, a complete conversion chain is implemented from pixel coordinates to Stonyhurst coordinates (using the sunpy.map.solar_pixelate_to_hpc() method) and then to Carrington coordinates (based on the astropy.coordinates.SkyCoord

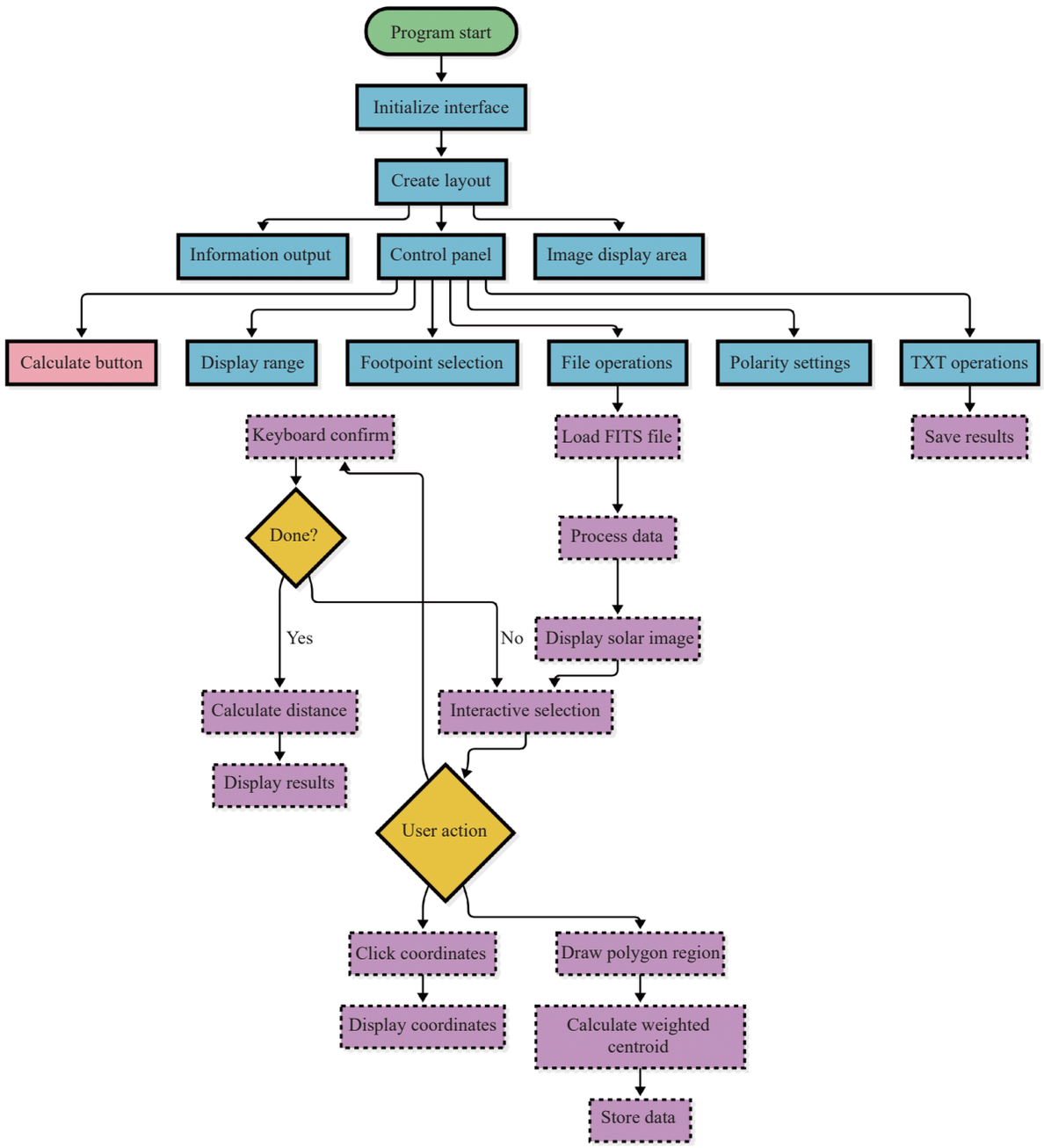

Fig. 1. Software flowchart illustrating the calculation workflow.

class). The conversion relationship can be expressed as $R_{\mathrm{Carrington}} = f(\phi_{\mathrm{Stony}}, t_{\mathrm{obs}})$.

To quantitatively characterize the spatial center of mass of magnetic flux distribution in solar ARs, we employ a magnetic flux-weighted centroid algorithm. This method determines the core weighted position of magnetic structures by calculating the spatial first-order moment of the absolute magnetic field values in ARs, avoiding the sensitivity of traditional morphological centroids to edge contours[11]. For a given AR domain Ω (typically defined by magnetogram threshold segmentation or manual selection), its weighted centroid coordinates $(x_{\mathrm{c}}, y_{\mathrm{c}})$ are defined as

$$(x_{\mathrm{c}}, y_{\mathrm{c}}) = \left(\frac{\sum\limits_{(x,\,y)\in\Omega} |B(x,\,y)| \cdot x}{\sum\limits_{(x,\,y)\in\Omega} |B(x,\,y)|}, \frac{\sum\limits_{(x,\,y)\in\Omega} |B(x,\,y)| \cdot y}{\sum\limits_{(x,\,y)\in\Omega} |B(x,\,y)|} \right), \quad (1)$$

where $B(x, y)$ represents the longitudinal magnetic field strength (in Gauss units) at pixel (x, y) within an AR. The absolute value operation ensures equivalent contributions to the centroid from both positive and negative polarities. The denominator $\sum\limits_{\Omega} |B(x,\,y)|$ represents the total absolute magnetic flux in region Ω, serving as a normalization factor. The numerator terms compute the weighted spa-

tial integrals of magnetic flux in the longitudinal (x) and latitudinal (y) directions, respectively.

The coordinates (x_c, y_c) physically characterize the core position of the magnetic flux distribution in the AR. Its calculation accuracy directly depends on the spatial resolution of the magnetogram (e.g., 0.5"/pixel for SDO/HMI) and the calibration level of magnetic field measurement errors.

To further suppress the influence of noise on the calculation of the magnetic flux-weighted centroid, we adopt a robust thresholding method based on the statistical properties of the quiet Sun region. This region is defined by customizing its range as areas within the full-disk magnetogram[12]. Within these regions, a root mean square (RMS) thresholding procedure is applied, specifically calculating the standard deviation (σ_{quiet}) of the magnetic flux values in the quiet Sun. A threshold value of $3\sigma_{\text{quiet}}$ is then used to exclude pixels whose magnetic flux falls below this value during the centroid computation.

This methodology is grounded in the statistical distribution of magnetic flux in the quiet Sun, where the flux is predominantly constituted by a small number of high-intensity magnetic elements, accounting for approximately 90% of the total flux while regions with low flux contribute minimally[13]. Therefore, discarding points with magnetic flux below $3\sigma_{\text{quiet}}$ does not lead to a significant loss of physical information. Instead, it substantially reduces noise-induced artifacts in the estimation of the magnetic flux-weighted centroid, thereby improving both the accuracy and reliability of the derived centroid position.

The thresholding procedure is described by

$$B_{\text{threshold}} = 3\sigma_{\text{quiet}}, \tag{2}$$

where σ_{quiet} is the standard deviation of the magnetic flux values in the identified quiet Sun regions. Only pixels satisfying

$$B(x,\ y) \geq B_{\text{threshold}}$$

are included in the summation of Equation (1).

To eliminate the impact of projection distortions (such as limb darkening and geometric distortions at the solar disk edges) in full-disk magnetograms on AR position measurements, it is necessary to convert Cartesian pixel coordinates (x, y) into standard heliographic spherical coordinates. Based on the spherical geometry of the Sun, the corrected heliographic latitude (θ) and longitude (ϕ) can be derived using World Coordinate System (WCS) parsing of FITS header parameters (e.g., CDELT1, CRVAL1) using sunpy.map.all_coordinates_from_map, followed by inverse projection transformation calculations,

$$\theta = \arcsin\left(\frac{y}{R_{\text{sun}}}\right),\ \ \phi = \arctan\left(\frac{x}{\sqrt{R_{\text{sun}}^2 - x^2 - y^2}}\right), \tag{3}$$

where R_{sun} is the apparent solar radius (in pixels), derived from the magnetogram calibration parameters, and x and y are Cartesian coordinates with the solar disk center as the origin, subject to the constraint $x^2 + y^2 \leq R_{\text{sun}}^2$. The latitude $\theta \in [-90°, 90°]$ (0° at the equator, positive northward) and longitude $\phi \in [-180°, 180°]$ (0° at the central meridian, positive westward).

The geometric interpretation of this transformation can be elucidated using two key steps related to coordinate calculation. For latitude calculation, the vertical offset y is first projected onto the normal component of the solar sphere, and this projected value is then mapped to the latitude angle using the arcsine function. For longitude calculation, the horizontal offset x is divided by the spherical curvature correction term $\sqrt{R_{\text{sun}}^2 - x^2 - y^2}$. This division operation yields the projected longitude angle on the tangential plane.

To standardize solar rotation observation data into the Carrington Coordinate System, the original Stonyhurst longitude must be converted to Carrington longitude. This transformation is achieved by adjusting the initial meridian offset and normalizing the longitude range, with the relationship,

$$L_{\text{car}} = (L_{\text{Stony}} - L_0 + 360°) \mod 360°. \tag{4}$$

To quantify the true spatial span of TL systems on the solar surface, it is necessary to calculate the great-circle distance between their two footpoints. This distance reflects the actual physical length of the magnetic loop crossing the equator and serves as a key parameter for analyzing the strength of trans-equatorial magnetic coupling[14,15].

Based on spherical trigonometry, the heliographic latitude-longitude coordinates of the two footpoints (θ_1, ϕ_1) and (θ_2, ϕ_2) are converted into a three-dimensional angular separation, calculated as

$$d = 2R_{\text{sun}} \arcsin\left(\sqrt{\sin^2\frac{\Delta\theta}{2} + \cos\theta_1 \cos\theta_2 \sin^2\frac{\Delta\phi}{2}}\right). \tag{5}$$

The results are given in both arcseconds (′ ′) and degrees (°) to accommodate diverse research requirements.

3. SOFTWARE DESIGN AND INNOVATIVE FEATURES

The software is designed with a layered architecture, consisting of three core layers with distinct functions. The Presentation Layer is built with Tkinter, and its primary role is to provide an intuitive GUI that includes functional modules such as file selection, coordinate system switching, and a results display area. The Logic Layer serves as the core processing component, implementing the magnetic map processing pipeline through the Pipeline class to execute key data processing tasks. The Visualization Layer uses Matplotlib for magnetic map dis-

play and annotation functions, facilitating the intuitive presentation of analysis results.

The software encompasses several key innovative features that enhance its usability and reliability for solar physics data analysis. First, it offers real-time coordinate synchronization: When users switch between different coordinate systems, the positions of magnetic flux-weighted centroids and coordinate grids are dynamically refreshed, ensuring that spatial information remains accurate and up-to-date throughout the operation. It also supports one-click export functionality, which allows users to export relevant data or results into files in either JSON or TXT format, streamlining the process of data sharing and subsequent analysis.

Using intelligent fault tolerance, via the sunpy.map.Map tool, the software can automatically detect invalid magnetic maps, and is equipped with an alert mechanism to notify users promptly of such issues, reducing the risk of erroneous data processing. To ensure the results are reproducible, end-to-end automation in the analysis workflow eliminates manual calculation errors commonly associated with traditional methods.

As shown in Table 1, comparative analysis with existing tools (IDL/SSW) demonstrates the significant advantages of PyTransHelio. It requires no programming skills, is open-source under the Massachusetts Institute of Technology (MIT) License, provides a dedicated TL analysis interface, and although its processing speed is currently "Medium (optimization in progress)", these features already outperform IDL/SSW, which lacks support for no-code operation, open-source licensing, and specialized analysis interfaces.

Table 1. A comparison of features of IDL/SSW and features of PyTransHelio tools

Feature	IDL/SSW	PyTransHelio
No programming skills required	✗	✓
Open-source license	✗	MIT license
Dedicated TLs analysis interface	✗	✓
Processing speed	Fast	Medium (optimization in progress)

4. VERIFICATION AND CASE STUDIES

4.1. Verification

A key distinction between PyTransHelio and conventionally used tools, such as IDL/SSW packages, lies in the calculation of Carrington longitudes. The Carrington longitude computations in IDL/SSW are based on earlier methodologies described on a dedicated webpage by the Space Physics Research Group (affiliated with the University of Maryland Department of Physics). This webpage was developed to organize and present observational data and charts from the Charge, Element, and Isotope Analysis System / Mass Time-Of-Flight (CELIAS/MTOF) Proton Monitor aboard the SOHO satellite, structured by Carrington Rotation. It notes that the initial IDL/SSW approach assumed a constant synodic rotation period of 27.2753 days for deriving Carrington rotation times. These techniques were later refined with sine-cosine series fits to align with *Astronomical Almanac* data, including a specific offset adjustment for 1996, to minimize residuals.

By contrast, PyTransHelio uses sunpy's implementation for Carrington coordinate calculations. As explicitly detailed on the same University of Maryland webpage, which contextualizes tool selection for analyzing SOHO/CELIAS/MTOF proton monitor data, sunpy-derived start and stop times of Carrington rotations closely match values from the *Astronomical Almanac*. Critically, the webpage explains that this sunpy-based methodology differs intentionally from the traditional approach used by IDL/SSW tools. This divergence in computational frameworks directly leads to the observed differences in Carrington longitudes.

To validate the accuracy of PyTransHelio in calculating Carrington coordinates and TL footpoint distances, we have conducted a comparative analysis against previously published studies using IDL/SSW-based methods (see Table 2). In this table, (S) shows southern hemisphere ARs, and (N) shows northern hemisphere ARs. Lat1 is the Carrington latitude of the TL footpoints derived from external research cases[10], while Lat2 shows the Carrington latitude of the TL footpoints obtained from our own data. (°)1 and (°)2 are the TL footpoint separations between our data and data from external sources. The results demonstrate strong consistency in derived Carrington latitudes and TL footpoint separations, with minor discrepancies attributable to the inherently qualitative nature of TL identification in existing literature, which often precludes high-precision quantitative comparisons. Notably, due to algorithmic differences in Carrington longitude calculations between IDL/SSW and sunpy (the underlying coordinate transformation library in PyTransHelio), longitudinal validation was instead performed against sunpy-based reference studies. As shown in Table 3 (TIME1 and LON1 are the eventtime and the corresponding Carrington longitude of the central meridian, as computed by the University of Maryland SpacePhysics Research Group. TIME2 and LON2 are our measured values, derived using PyTransHelio, for the same event times to facilitate a comparative assessment), the calculated Carrington longitudes of the central meridian at multiple observation epochs show excellent agreement with these benchmark values, further confirming the computational robustness of PyTransHelio.

Table 2. Comparison between PyTransHelio and other IDL/SSW-based TL studies

Date	AR (N)	Lat1 (N)	Lat2 (N)	AR (S)	Lat1 (S)	Lat2 (S)	(°)1	(°)2
2011−02−14	0	10.5	6.14	11158	−11.7	−19.13	24.2	30.291
2011−03−13	0	12.8	6.26	11171	−10.5	−15.92	23.7	27.735
2011−04−18	11191	10.6	7.55	0	−7.1	−14.19	17.8	21.766
2011−05−23	0	15.9	14.3	11216	−10.7	−20.2	27.2	34.967
2011−10−16	11319	3.7	9.59	11316	−13.7	−11.92	17.5	21.543
2012−06−15	11506	8.3	11.78	11504	−12.9	−15.71	21.8	28.782
2012−07−03	11513	11.2	15.85	11515	−13.5	−15.99	25.6	33.831
2013−03−09	0	17	8.06	11689	−8.9	−12.11	26.1	25.138
2013−04−04	11708	14.3	10.74	11711	−5.4	−18.03	22.3	34.276
2017−05−20	12656	14.7	11.91	12658	0.2	−6.99	15.4	18.960

Table 3. Comparison of Carrington longitudes of the central meridian at different event times

TIME1	LON1	TIME2	LON2
1996−05−05 10:00:00	356.2	1996−05−05 10:39:04	351.4
1999−07−22 11:00:00	353.5	1999−07−22 11:39:00	346.4
2001−01−18 11:00:00	346.9	2001−01−18 11:15:01	340.8
2004−12−07 00:00:00	344.2	2004−12−07 00:00:28	343.2
2013−10−08 00:00:00	229.8	2013−10−08 00:58:17	229.3
2016−01−08 00:00:00	182.3	2016−01−07 23:58:08	181.8
2021−11−05 00:00:00	173.8	2021−11−04 23:58:33	173.5

4.2. Data Preparation

Before using our program for trans-equatorial loop analysis, we need to configure the environment and obtain FITS files of Line-of-Sight (LOS) magnetograms and X-ray images from astronomy databases. For the tested FITS files available for software analysis, information about their source (i.e., the instrument and satellite of origin) and download links can be found in Table 4.

Table 4. Data sources for magnetograms and X-ray images

Data type	Satellite	Instrument	Data download link
LOS magnetogram sources	SDO	HMI	NASA SDO
	SOHO	MDI	ESA SOHO
X-ray image sources	Yohkoh	SXT	NASA Yohkoh data archive
	Hinode	XRT	Hinode data center

It should be noted that X-ray images are not directly loaded into the program. Instead, the user needs to determine the footpoint positions of trans-equatorial loops by comparing magnetograms and X-ray images recorded on the same day (with a recommended time difference of no more than 12 h) before using the program for analysis.

Both SOHO/MDI and SDO/HMI are used to obtain solar LOS magnetograms, but they differ significantly in technical parameters, resolution, and application scenarios. Their specific characteristics and uses are shown in Table 5.

Although this program has a partial header keyword completion function, when downloading FITS files of LOS magnetograms from online databases, it is still recommended to select versions with more complete information (e.g., when downloading SOHO/MDI FITS files, the user should select "ALL" for keywords, as shown in Fig. 2). This is because sunpy requires the header of a FITS file to contain key information for analysis (detailed in Table 6).

Because X-ray images from different years were observed by different satellites and instruments, the download process may be complicated. Therefore, it is recommended to use HelioViewer[①], which integrates X-ray images from various instruments across all time periods, facilitating quick access to X-ray images of specific dates.

4.3. Environment Configuration

First, ensure that the Python version is ⩾3.11, then install all third-party libraries listed in the requirements.txt file in the code repository, using the pip command. For a more detailed configuration guide, refer to the documentation of PyTransHelio.

After completing the above steps, the program is ready to be launched. To access the software via command line, users should first navigate to the program directory using the cd command, then execute the program by

1. HelioViewer website: *https://helioviewer.org/*

Table 5. Comparison of SOHO/MDI and SDO/HMI instrument characteristics

Satellite/Instrument	Magnetogram characteristics	Primary scientific applications
SOHO/MDI	– Spatial resolution: 2" – Temporal cadence: 96 min – Spectral line: Fe I 676.8 nm (photospheric) – Limitations: Low SNR (10^{-3} T sensitivity), limited dynamic range; struggles with weak-field regions (e.g., internetwork)	– Long-term evolution of solar magnetic fields (SC 23) – Sunspot dynamics and AR monitoring – Ground truth for pre-2010 magnetogram calibrations
SDO/HMI	– Spatial resolution: 0.5" – Temporal cadence: 12 min – Spectral line: Fe I 617.3 nm – Advantages: High sensitivity (detects < 1 G fields), full Stokes vector measurements	– Real-time space weather forecasting (flares/CMEs) – Quantitative coronal magnetic field extrapolations – Small-scale flux emergence/dispersal studies

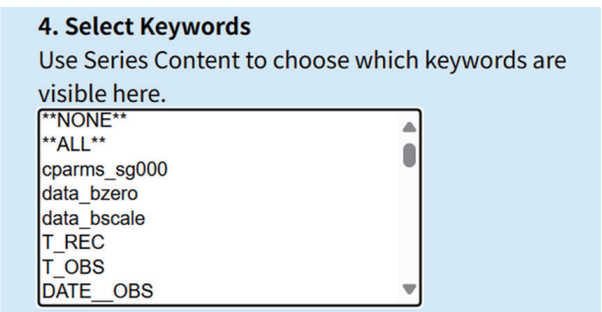

Fig. 2. Example of the SOHO/MDI FITS download interface, showing the keyword selection option. "ALL" should be selected here to ensure complete header information.

entering python PyTransHelio.py in the command line interface. For those using an integrated development environment (IDE), the program can be started directly by clicking the built-in run button.

4.4. Case Study

(1) Click "Select FITS file" to choose the FITS file for analysis. You will then enter the file selection page. Navigate to your FITS file directory by clicking, then double-click the FITS file to select it.

Fig. 3 shows the appearance of magnetograms from SDO/HMI and SOHO/MDI when opened in the software. The two appear almost identical, except that SDO/HMI magnetograms have higher resolution (4096 × 4096 pixels), which correspondingly makes the software analysis slightly slower. By contrast, MDI has a lower resolution (1024 × 1024 pixels), resulting in faster software analysis.

Table 6. Required FITS header keywords for solar magnetogram analysis, and essential metadata fields that must be present in FITS file headers for correct processing

Keyword	Description
CTYPE1, CTYPE2	Coordinate types (e.g., 'HPLN-TAN' for heliographic longitude, 'HPLT-TAN' for heliographic latitude)
CUNIT1, CUNIT2	Coordinate units (e.g., 'arcsec')
CRPIX1, CRPIX2	Positions of reference pixels in the image
CRVAL1, CRVAL2	Physical coordinate values corresponding to reference pixels (e.g., central longitude/latitude of the solar disk)
CDELT1, CDELT2	Pixel scale (e.g., 1.0"/pixel)
DSUN_OBS	Sun-Earth distance (unit: m)
RSUN_OBS	Apparent radius (unit: arcsecond)

(2) As shown in Fig. 4A, a set of interactive controls is located below the "Select File" button, consisting of two rows of spinner controls. The first row contains a pair of spinners that allow the user to adjust the upper and lower bounds for the visualization of magnetic flux values in the magnetogram. A smaller interval between these bounds enhances the contrast of high-flux regions, making them more distinguishable, while a larger interval reduces the contrast and thus the visibility of such structures.

The spinner labeled "Noise Threshold" in the second row is used to suppress the contribution of weak magnetic field noise during the subsequent computation of the magnetic flux-weighted centroid. Specifically, pixels with magnetic flux values below this threshold are excluded from the calculation.

(3) After completing the aforementioned two steps, the user should select the "quiet region" radio button (see Fig 4A). This region corresponds to areas characterized by generally low magnetic flux density, which typically appear as relatively uniform gray patches in the magnetogram, without significant concentrations of black or white pixels. The user should then move the cursor to the magnetogram display and delineate such a quiet Sun region by tracing a polygonal contour (see Fig 5).

On closing the polygon, the value in the "noise threshold" spinner control will update automatically. This updated value represents the calculated threshold, based on Equation (2), which uses the statistical properties of the selected quiet region. During the subsequent computa-

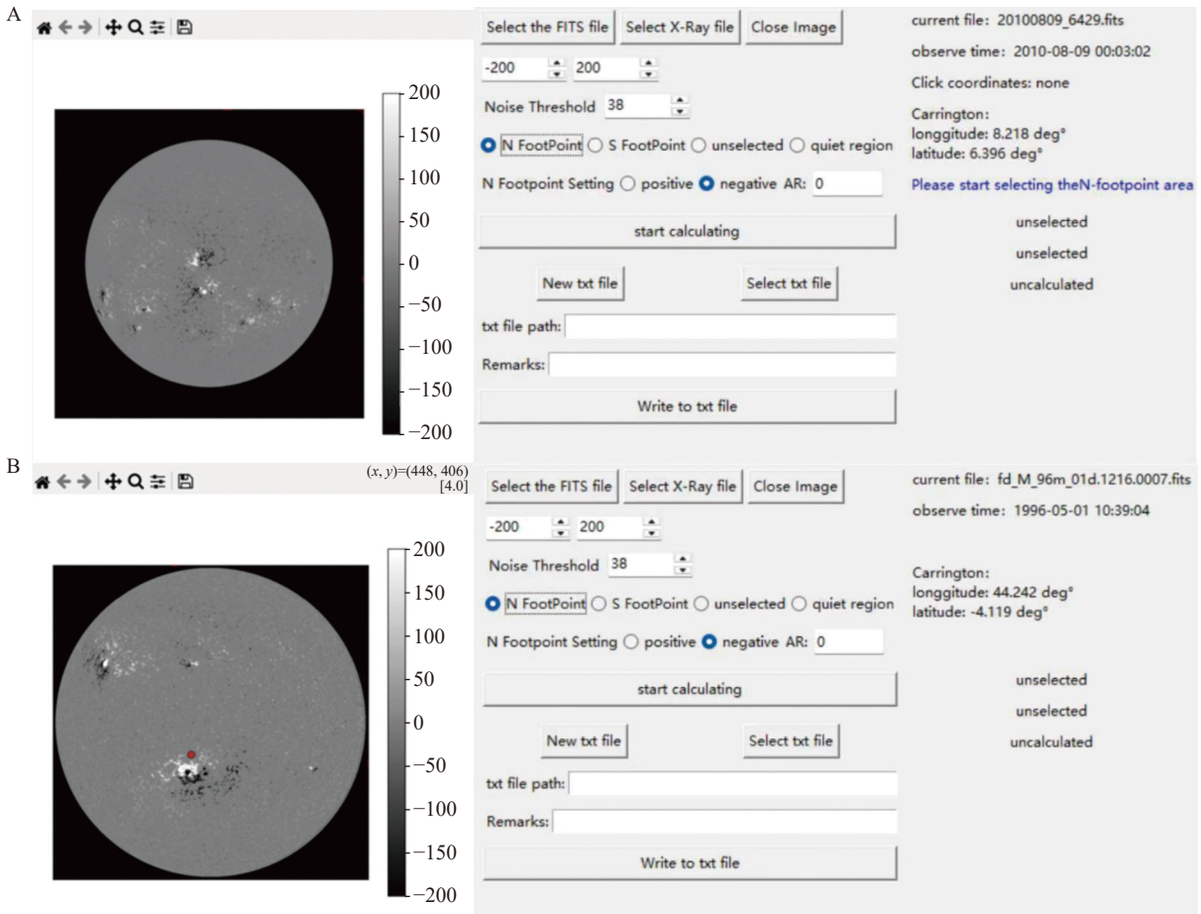

Fig. 3. (A) SDO/HMI magnetogram showing the appearance when opened in the software (at a resolution of 4096 × 4096 pixels). (B) SOHO/MDI magnetogram showing the appearance when opened in the software (at a resolution of 1024 × 1024 pixels).

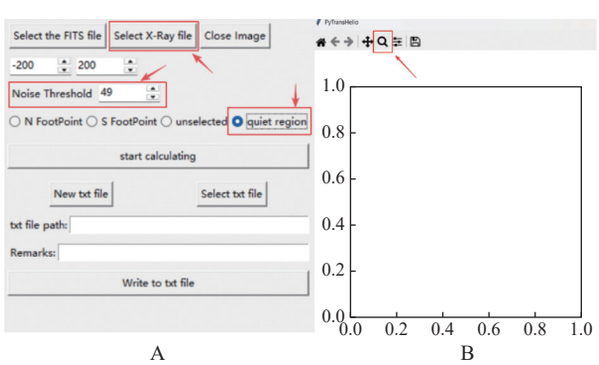

Fig. 4. (A) Positions of "noise threshold", "select X-Ray file", and "quiet region". (B) Magnifying Glass Button interface element for activating zoom functionality.

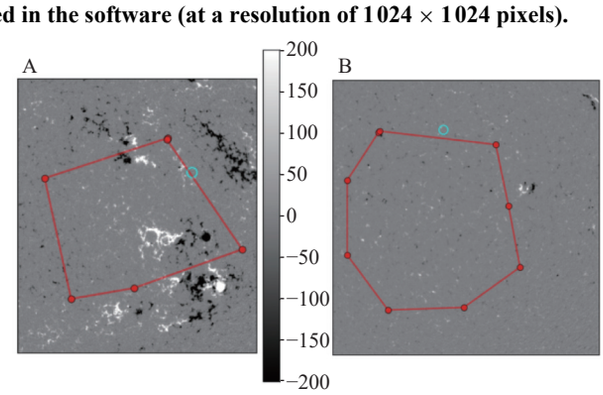

Fig. 5. A comparison of the selected areas shows that suitability as a quiet region depends on the concentration of black or white pixels. (A) Unsuitable−characterized by considerable concentrations of black or white pixels. (B) Suitable−characterized by the absence of significant black or white pixels.

tion of the magnetic flux-weighted centroid, pixels with magnetic flux values below this threshold will be excluded from the calculation.

(4) Locate the footpoints of trans-equatorial loops in X-ray images and map them to approximate positions in full-disk magnetograms (Fig. 6).

Currently, the software supports X-ray image files in two formats only: .fts (used by Yohkoh/SXT) and .fits (used by Hinode/XRT). Users may load locally stored files in either format via the "Select X-ray File" button on the graphical interface (Fig. 4A). This functionality facilitates direct visual comparison between AR locations in the magnetogram and the corresponding X-ray image (Fig. 7).

The program automatically extracts and compares the observation timestamps from the headers of both the magnetogram and the X-ray file. A green "Time Matching" indicator is displayed if the absolute time difference is less than

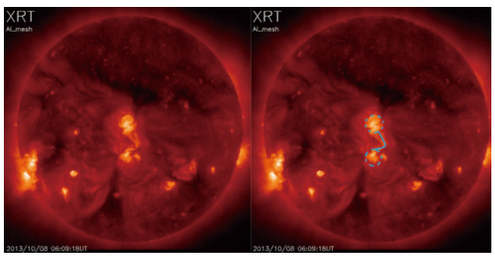

Fig. 6. A composite figure showcasing coronal structures in X-ray. The left image highlights the approximate positions of identified footpoints, while the right image displays TLs with key locations marked.

12 h (see Fig. 8A). This temporal matching condition minimizes positional discrepancies of solar features between the two images, reducing the potential for human error in misalignment.

(5) Click the "Magnifying glass" button (Fig. 4B) to zoom in on a specific region for detailed observation, facilitating subsequent AR selection (Fig. 9B).

Clicking the "Magnifying glass" button enables zoom operations on the image. This feature allows users to conveniently magnify specific areas for clearer observation of image details, facilitating more precise selection of regions of interest in subsequent steps. After zooming in, image details become more prominent, making it easier for users to identify and locate relevant features.

(6) Ensure no top toolbar buttons are selected (Fig. 10, distinguished by the depressed appearance when selected), then drag to outline the target AR (Fig. 9A).

When the polygon closes, pressing "Enter" will display the AR ID, the magnetic flux-weighted centroid coordinates in three coordinate systems (shown on the right panel), and a dark blue cross marking the centroid position in the preview image. The right panel includes several options: polarity (with choices of Positive or Negative), hemisphere (with options of North or South), an input field for the AR ID, and N FootPoint thresholds featuring custom flux limits with automatically set default values.

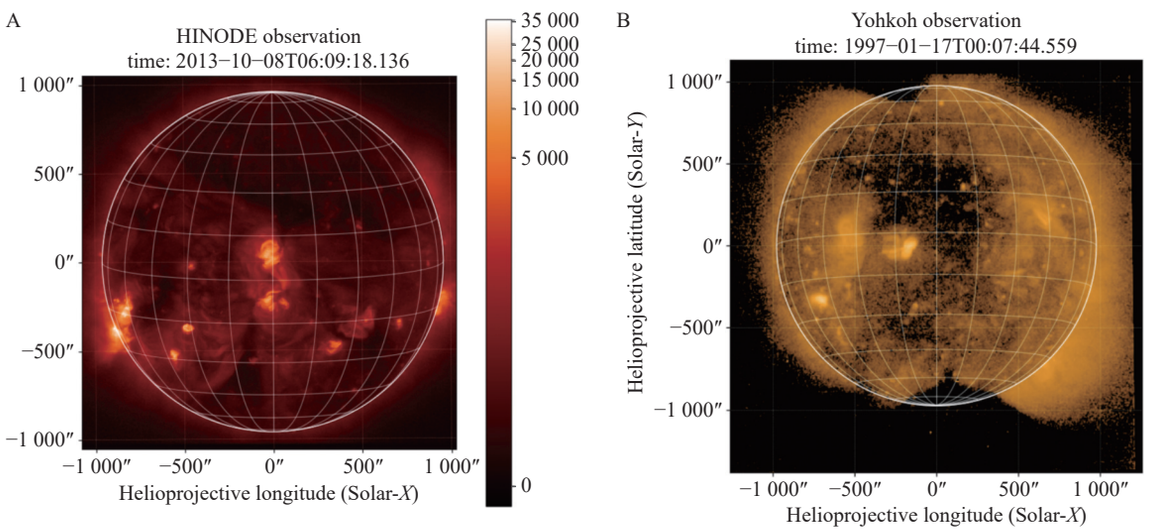

Fig. 7. Comparison of X-ray images of the Sun from Hinode/XRT (A) and Yohkoh/SXT (B).

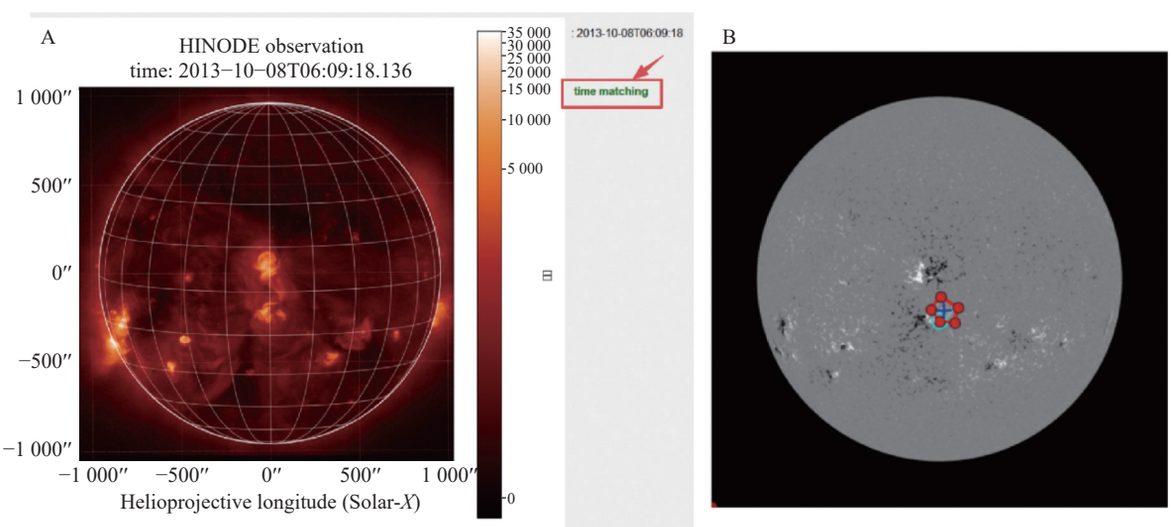

Fig. 8. (A) Position of "time matching". (B) Full-disk view after returning from region selection.

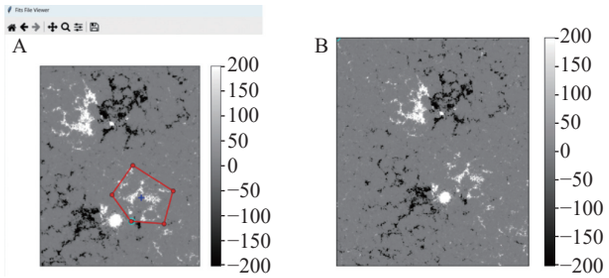

Fig. 9. (A) AR outline created by dragging to select the target region. (B) Zoomed region view showing enhanced details for AR selection.

Fig. 10. Visual contrast of a toolbar button in its unselected (top) and selected, depressed (bottom) states.

(7) If returning to full-disk view after selecting a southern hemisphere region, click the "Left arrow" button (Fig. 8B shows the returned view).

(8) Repeat the process to calculate the magnetic flux-weighted centroid for the opposite polarity region (Fig. 11A).

A green confirmation message will appear when selections are complete (Fig. 11B). To export the results, users can either click "Start calculating" and then "Select TXT" to append the results to an existing file, or choose "New TXT" to save the results to the desktop with automatically generated headers.

In the output sample (Fig. 12), the meanings represented by each abbreviation are: NPOL & SPOL are polarity of northern and southern footpoints (north/south polarity); NARN & SARN, are AR numbers for northern and southern footpoints (AR number); NLON/NLAT & SLON/SLAT are Carrington longitude and latitude of northern and southern ARs; LDEG & LRAD are Footpoint separation distance of TL, but with different units (length degree & length radian); and REMARK is for additional notes.

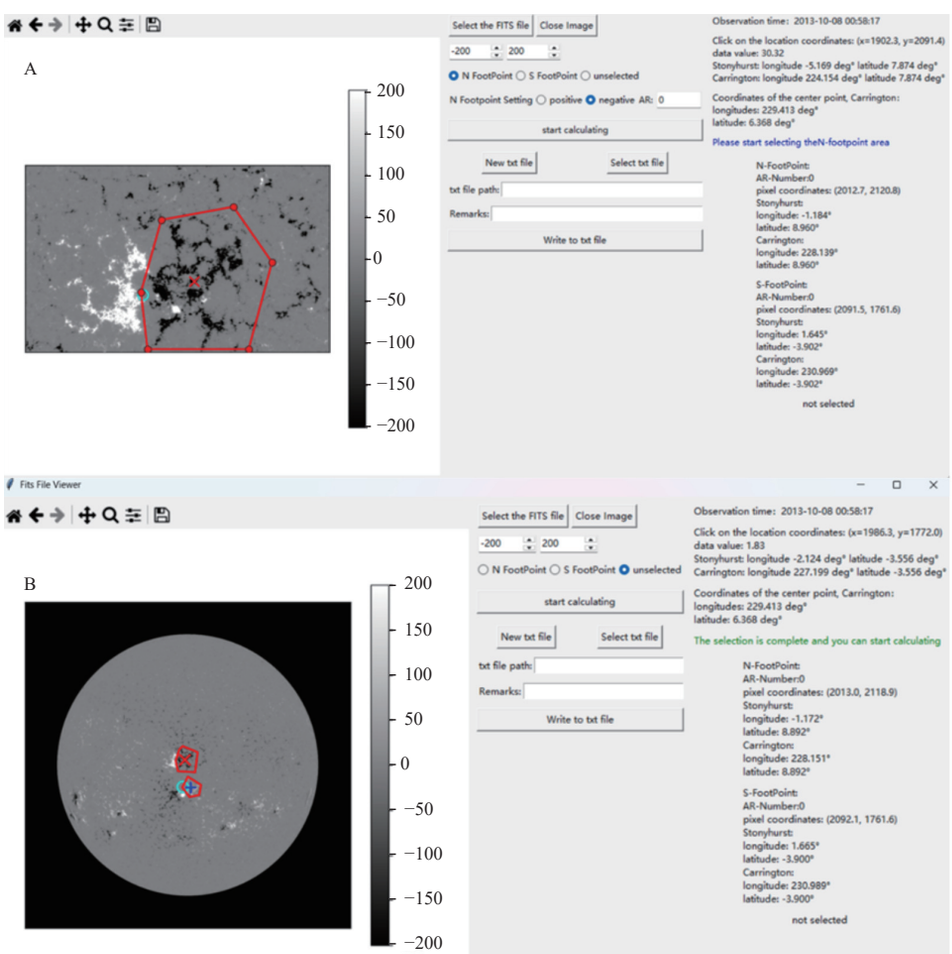

Fig. 11. (A) Opposite polarity region selection with centroid calculation. (B) Confirmation message showing ready state for calculation.

DATE	NPOL	NARN	NLON	NLAT	SPOL	SARN	SLON	SLAT	LDEG	LRAD	REMARK
20131008	-	11856	229.22	10.31	+	11857	230.91	-3.79	14.198	0.248	

Fig. 12. A sample of the TL parameters output saved in a text file (.txt) by the software.

These specific parameter combinations are important in solar physics research and space weather forecasting[4], aiding in identifying and studying TLs, where the posi-

tive/negative characteristics of NLAT and SLAT directly reflect trans-equatorial properties. NPOL/SPOL, NARN/SARN, and NLON/SLON comprehensively describe the specific magnetic field structures and source regions connecting the two hemispheres, while LDEG/LRAD quantifies the scale of these trans-equatorial connections.

In terms of space weather, trans-equatorial loops, as regions of complex magnetic field structures, are prone to energy accumulation and can trigger eruptive events such as flares and CMEs[16]. These parameters enable determination of whether eruptive events involve trans-equatorial loops (based on NARN/SARN, NPOL/SPOL, NLON/NLAT/SLON/SLAT) for event attribution, and monitoring of the evolution of trans-equatorial loops (such as scale changes or increased complexity in the footpoint ARs) to assess their instability and provide clues for predicting potential eruptive events.

The quantifiable magnetic loop scale parameters provided by LDEG and LRAD facilitate statistical analyses, such as studying typical scale distributions of trans-equatorial loops and their relationship with SC phases, as well as physical modeling, such as calculating magnetic energy. Additionally, standardized output information, including AR numbers, Carrington coordinates, polarity, separation distance, and remarks, ensures clear and comparable analysis results, making them easier for other researchers to understand and use, thereby promoting data sharing and reproducibility in scientific research.

5. DISCUSSION AND FUTURE DIRECTIONS

PyTransHelio's capability is most evident in its automated workflow and scalable architecture. This capability, rigorously validated with data from established instruments including SDO/HMI, SOHO/MDI, YOHKOH/SXT, and Hinode/SRT, provides a robust foundation for integrating data from future missions. Preliminary assessment suggests its architecture may potentially support data from new instruments, like Solar Orbiter Polarimetric and Helioseismic Imager (PHI), pending formal compatibility verification of the specific FITS formats it uses. This positions the framework as a promising cornerstone for future solar physics research. In the context of AR studies, the ability of our software to rapidly process and analyze data is invaluable. For example, during the peak of a SC, when the frequency and complexity of ARs are expected to increase[17], PyTransHelio can assist in quickly identification and characterization of ARs, enabling researchers to monitor their magnetic evolution in real-time. This real-time monitoring can provide early warnings for potential solar eruptions, such as flares and CMEs, which can have significant impacts on Earth's space environment[18,19].

Our tool also holds great educational potential. By providing an intuitive and user-friendly interface, PyTransHelio can introduce students and novice researchers to the complex world of solar physics. Through hands-on experience with analyzing ARs and TLs, learners can gain a deeper understanding of the underlying physical processes. This educational aspect is further enhanced by the open-source collaboration model. The GitHub repository serves as a platform for the community to contribute, share ideas, and further improve software. Such a collaborative effort can lead to the development of new features and improvements, making PyTransHelio an even more powerful tool for solar physics education and research.

Like any scientific tool, PyTransHelio also has its limitations. In weak magnetic field regions, the detection noise remains a challenge. To address this, future work will focus on implementing advanced segmentation models using artificial intelligence. These models can potentially enhance the accuracy of magnetic field detection, allowing for more precise analysis of ARs in these regions. Additionally, the processing speed for large datasets is an area of concern. With the increasing volume of solar data being collected, optimizing the tool's multithreading capabilities is essential. By improving the processing speed, PyTransHelio can handle larger datasets more efficiently, enabling researchers to analyze more comprehensive datasets and draw more accurate conclusions about ARs and TLs.

In terms of community impact, PyTransHelio is an important addition to the PyData solar physics ecosystem. As a complementary tool, it encourages researchers to adopt and contribute to its development. By using PyTransHelio, researchers can streamline their workflows, making their research more efficient. Moreover, the open-source nature of the tool promotes collaboration, allowing researchers from different backgrounds to work together. This collaborative environment can lead to new discoveries and advancements in solar physics, particularly in the study of ARs and their associated phenomena.

Our software's innovation is its ability to encapsulate professional astronomical data processing capabilities with intuitive click-based operations, significantly lowering barriers to research entry. We anticipate that it will emerge as a valuable asset for both solar physics education and research, and we warmly invite the community to engage in its testing and usage.

ACKNOWLEDGEMENTS

This work is supported by the National Key R&D Program of China (2021YFA1600501), National Natural Science Foundation of China (12373057), ISSI/ISSI-BJ Team 2024 (24-604), and the Chinese Meridian Project (CMP). Marianna B. Korsós is grateful for the Leverhulme Trust Found (ECF-2023-271). Marianna B. Korsós and Robertus Erdélyi acknowledge the Nemzeti Kutatási, Fejlesztési és Innovációs Hivatal (NKFIH) OTKA (K142987). Robertus Erdélyi is grateful to Science and Technology Facilities Council UK (STFC, ST/M000826/1), and acknowledges the President's International Fellowship Initiative in

China (2024PVA0043) and the NKFIH Excellence Grant (TKP2021-NKTA-64) for enabling this research.

AUTHOR CONTRIBUTIONS

Silin Liu carried out program debugging and manuscript writing. Jie Chen took charge of steering the team's research direction, coordinating project advancement, and proposing core research topics. Zechen Wen and Chenfei Zhao accomplished the derivation of the main algorithm for this program and provided test cases. Zihan Yu conducted comparative studies with the old methods (IDL/SSW). Robertus Erdélyi, Marianna B. Korsós, and Ying Song contributed to the conceptualization of the research framework; provided methodology validation for the comparative analysis; offered critical review and editing input that significantly enhanced the intellectual content and clarity of the manuscript; and supervised the overall research activity. All authors have read and approved the final manuscript.

AI DISCLOSURE STATEMENT

Deepseek and Doubao AI were employed specifically for translating sentences with uncertain terminology and polishing certain parts of the article content to enhance academic rigor and logical coherence. The authors have meticulously verified the accuracy of the texts generated or optimized by these two AI tools through both manual review and cross-referencing with relevant literature. It should be emphasized that the application of the aforementioned AI tools did not involve the core parts of the paper (including but not limited to research hypotheses, experimental design, data analysis, and conclusion derivation). The authors carefully reviewed, edited, and revised the AI-generated/optimized texts to their own preferences, assuming ultimate responsibility for the content of the publication.

DATA AND CODE AVAILABILITY

The project is open-sourced on GitHub (PyTransHelio repository) with pip-installable releases. Runtime environment requirements ensure version dependency transparency. Detailed installation guides and user manuals are included in the project documentation to guarantee reproducibility.

DECLARATION OF INTERESTS

Initial empty paragraph

REFERENCES

[1] Wang, Z. F., Jiang, J., Zhang, J., et al. 2020. Activity complexes and a prominent poleward surge during solar cycle 24. *The Astrophysical Journal*, **904**(1): 62.

[2] McIntosh, S. W., Leamon, R. J. 2014. On magnetic activity band Overlap, interaction, and the formation of complex solar active regions. *The Astrophysical Journal*, **796**(1): L19.

[3] Jaswal, P., Sinha, S., Nandy, D. 2025. Deconstructing the Properties of Solar Super Active Region 13664 in the Context of the Historic Geomagnetic Storm of 2024 May 10-11. *The Astrophysical Journal*, **979**(1): 31.

[4] Bobra, M. G., Sun, X., Hoeksema, J. T., et al. 2014. The Helioseismic and Magnetic Imager (HMI) vector magnetic field pipeline: SHARPs–space-weather HMI active region patches. *Solar Physics*, **289**(9): 3549−3578.

[5] Lin, J. 2007. Observational features of large-scale structures as revealed by the catastrophe model of solar eruptions. *Chinese Journal of Astronomy and Astrophysics*, **7**(4): 457−476.

[6] Korsos, M. B., Ruderman, M. S., Erdelyi, R. 2018. An application of the weighted horizontal magnetic gradient to solar compact and eruptive events. *Advances in Space Research*, **61**(2): 595−602.

[7] Simunac, K. D. C., Galvin, A. B., Farrugia, C. J., et al. 2012. The heliospheric plasma sheet observed in Situ by three spacecraft over four solar rotations. *Solar Physics*, **281**(1): 423−447.

[8] Jiang, J., Choudhuri, A. R., Wang, J. X. 2007. A new explanation for the origin of trans-equatorial loops based on a dynamo model. *Solar Physics*, **245**(1): 19−25.

[9] Chen, J., Bao, S. D., Zhang, H. Q. 2006. A statistical study of transequatorial loops. *Solar Physics*, **235**(1-2): 281−294.

[10] Yu, Z. H., Chen, J., Liu, J. H., et al. 2023. A statistical study of trans-equatorial loops from 2006 to 2020. *Monthly Notices of the Royal Astronomical Society*, **524**(4): 5880−5890.

[11] Martinez Pillet, V., Lites, B. W., Skumanich, A. 1997. Active region magnetic fields. I. Plage fields. *The Astrophysical Journal*, **474**(2): 810−842.

[12] Lites, B. W., Kubo, M., Socas-Navarro, H., et al. 2008. The horizontal magnetic flux of the quiet-Sun internetwork as observed with the hinode spectro polarimeter. *The Astrophysical Journal*, **672**(2): 1237−1253.

[13] Stein, R. F., Nordlund, Å. 2012. On the formation of active regions. *The Astrophysical Journal*, **753**(1): L13.

[14] Long, D. M., Valori, G., Pérez-Suárez, D., et al. 2017. Measuring the magnetic field of a trans-equatorial loop system using coronal seismology. *Astronomy & Astrophysics*, **603**: A101.

[15] Wang, J. X., Zhang, Y. Z., Zhou, G. P., et al. 2007. Solar trans-equatorial activity. *Solar Physics*, **244**: 75−94.

[16] Khan, J. I., Hudson, H. S. 2000. Homologous sudden disappearances of transequatorial interconnecting loops in the solar corona. *Geophysical Research Letters*, **27**(8): 1083−1086.

[17] van Driel-Gesztelyi, L., Green, L. M. 2015. Evolution of active regions. *Living Reviews in Solar Physics*, **12**(1): 1.

[18] Delannée, C., Aulanier, G. 1999. CME associated with transequatorial loops and a bald patch flare. *Solar Physics*, **190**(1): 107−129.

[19] Teng, W. L., Su, Y. N., Ji, H. S., et al. 2024. Unexpected major geomagnetic storm caused by faint eruption of a solar trans-equatorial flux rope. *Nature Communications*, **15**(1): 9198.